Microstructure and mechanical property evolutions of bulk core-shell structured Ti-N alloys during annealing

Y.S. Zhang [a], W. Zhang [a], X. Wang [a], J.W. Lu [a], Y.H. Zhao [b], *

[a] Northwest Institute for Nonferrous Metal Research, Xi'an, Shanxi, 710016, China
[b] Nano Structural Materials Center, School of Materials Science and Engineering, Nanjing University of Science and Engineering, Nanjing, 210094, China

ABSTRACT

Bulk dense core-shell structured Ti-N alloys with three different N contents were synthesized, and then annealed at different temperatures to tailor the mechanical performances. Compression tests show that with increasing N content (nitriding temperature and time), the Ti-N shell thickness and yield strength increase (from 0.9 to 1.2 GPa) with a decrease in fracture plasticity (from 27% to 3%). With increasing annealing temperature, the Ti-N shell thickness and yield strength first increase and then decrease, while fracture plasticity remains unchanged except a dramatic drop at 1500 °C. There exists a linear relationship between the yield strength and shell area fraction indicating the hardening effect of the Ti-N shell.

© 2017 Elsevier B.V. All rights reserved.

1. Introduction

Ti and its alloys have been widely used in aerospace, chemical and bio-medical fields due to their high specific strength and high corrosion resistance as well as excellent fracture toughness [1,2]. The wide engineering applications invoke the widespread research on microstructures and properties of Ti alloys [3–5].

It has been always the seeking aim for materials scientists to design advanced structural alloys or composites with both high strength and high toughness by tailoring their microstructures. The gradient nano-grained/coarse-grained architecture has recently been verified by numerous experimental results to be an effective route to achieve a superior combination of high strength and good ductility [6,7]. Laminated Ti–TiBw/Ti composite containing both Ti layers and TiBw/Ti composite layers exhibited a much enhanced strength-ductility synergy (an ultimate tensile strength of 625 MPa and an elongation of 19%) compared with conventional monolithic TiBw/Ti composite (720 MPa, 7.5%) [8]. The interpenetrating Mg–TiNi composites exhibited the greatly improved mechanical properties: 10 vol% TiNi addition increases yield strength by 36% and ductility from 14.5% to 20% [9].

Recently, a novel network reinforcement architecture in TiBw/Ti-6Al-4V composite was synthesized exploiting superior mechanical performances [10]. In this microstructure, the quasi-continuous and stronger network boundary phase strengthens the composite and the softer matrix phase toughens the composites, simultaneously. In our previous study, a bulk core-shell (CS) structured Ti alloy with a similar network distribution of reinforcement, constituted by isolated soft coarse-grained (CG) Ti cores and hard Ti-N solid solution shells by means of spark plasma sintering (SPS) of nitrided Ti particles has been fabricated successfully [11]. In this study, CS Ti alloys with three different shell thicknesses were synthesized by altering nitriding conditions as well as the N contents. One of them was characterized by a discontinuous CS structure. The CS Ti alloys were then annealed at different temperatures, and the mechanical behaviors with respect to the variations in microstructure, especially the shell thickness were discussed.

2. Experimental

Commercial pure (CP) Ti powder with particle size distribution ranging from 150 μm to 250 μm was chose as the feedstock. Before nitriding process, the Ti powder was first encapsulated in a porous stainless steel mould which could rotate during nitriding to make a homogeneous reaction. Ti powder in the steel mould was then put

in a tube furnace with N atmosphere and three batches of nitriding experiments were conducted at 900 °C for 15 min, and 1000 °C for 15 min and 30 min, respectively, and the corresponding compacts are denoted as Ti-900-15, Ti-1000-15 and Ti-1000-30 in subsequent context for conciseness. After nitriding, the Ti power was air cooled to room temperature. The nitrided Ti powder was sintered by using a SPS machine (Elenix company, Japan) in a vacuum of 10^{-1} Pa. Before SPS, the nitrided Ti powder was packed into a cylindrical graphite die with an inner diameter of 30 mm. By controlling the electric current at a range of 2000−3000 A and a voltage range of 5−10 V, SPS was conducted at 1100 °C for Ti-900-15 and Ti-1000-15, 1200 °C for Ti-1000-30 at a heating rate of about 150 °C/min under a pressure of 40 MPa and duration of 5 min. After sintering, the load was removed, and the furnace was cooled.

Microstructure characterizations and metallographic analysis were performed by using an optical microscope (OM, Leica MPS 30) and a transmission electron microscopy (TEM) on a JEOL 2010 microscope operated at a voltage of 200 kV. For OM observations, the samples were mechanically polished via a standard metallographic procedure and subsequently etched using a solution of $HF:HNO_3:H_2O = 1:1:3$ in volume. Thin foil samples for TEM observations were cut from the samples and thinned by ion thinning at low temperatures. The lateral morphology observations for compression specimen and compositional analysis were conducted on a JXA-8230 electro probe (EP).

Annealing treatments to the compacts were conducted at temperatures of 1000 °C, 1100 °C, 1300 °C and 1500 °C for 1 h in a vacuum of 1×10^{-3} Pa. The contents of oxygen and N were analyzed by using a carrier gas hot extraction (O/N analyzer/Leco) to be 0.11 wt% O, 0.44 wt% N for Ti-900 and 0.12 wt% O, 0.95 wt% N for Ti-1000-15, 0.12 wt% O, 1.45 wt% N for Ti-1000-30 compacts.

Room-temperature mechanical properties were characterized under quasi-static uniaxial compression loading by using a conventional CMT5105 mechanical testing system at a strain rate of $5 \times 10^{-4}\,s^{-1}$. Compression samples with sizes of 3 mm in diameter and 6 mm in length were cut from the sintered specimens according to ASTM (American society for testing and materials) standards. Commercial pure Ti (CP Ti) compact was also conducted under the same conditions for comparison.

3. Results and discussion

Fig. 1a−c are optical images of the as-sintered Ti-900-15, Ti-1000-15 and Ti-1000-30 specimens. Full densified compacts are obtained without any pores. Moreover, the compacts show a unique feature, constituted by numerous networked CS structural cells with the size comparable to that of the as-received particles. The three samples differ in the shell thickness. It is noted that the network architecture is discontinuous in Ti-900-15. With N content (nitriding temperature and time) increasing, the CS network becomes more prominent with an increasing shell thickness. The EP line analysis shows the enrichment of N in the shell as compared to the core (Fig. 1d). Typical bright field TEM micrograph and selected area diffraction (SAD) patterns in Fig. 1e confirm that both the core and shell are α-Ti with a sharp CS boundary. It can be concluded that the core is α-Ti with low N interstitial content and the shell is the N solid solution phase. The detailed formation mechanisms of the CS Ti-N alloys were analyzed in our previous work [11]. Briefly, during sintering, the Ti core experiences a $\alpha \rightarrow \beta$ phase transformation while the Ti-N shell keeps α status due to the high N concentration, thus forming a α/β phase boundary [11]. Such a CS structure is remained when cooling down to room temperature,
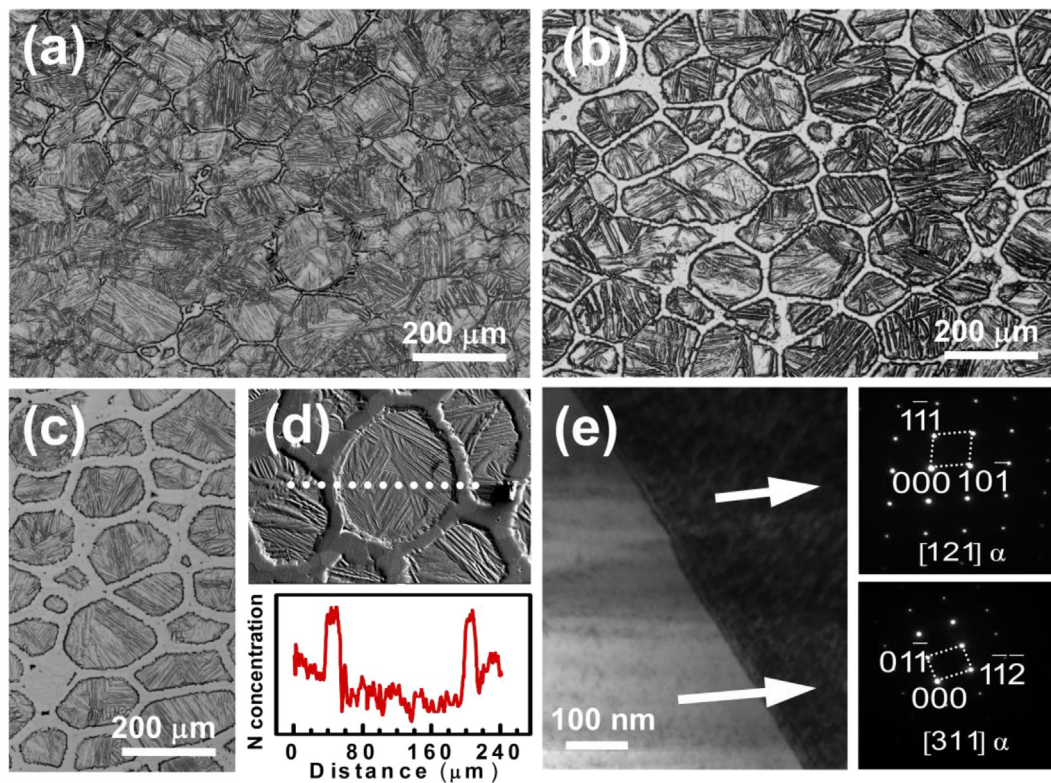
Fig. 1. Optical images of the SPS sintered specimens: (a) Ti-900-15, (b) Ti-1000-15, (c) Ti-1000-30, and (d) EP image and EP analysis of N concentration along the white dotted line in the EP image of Ti-1000-30, (e) bright field TEM image and selected area diffraction (SAD) patterns corresponding to core and shell regions along [121] and [311] zone axis, respectively.
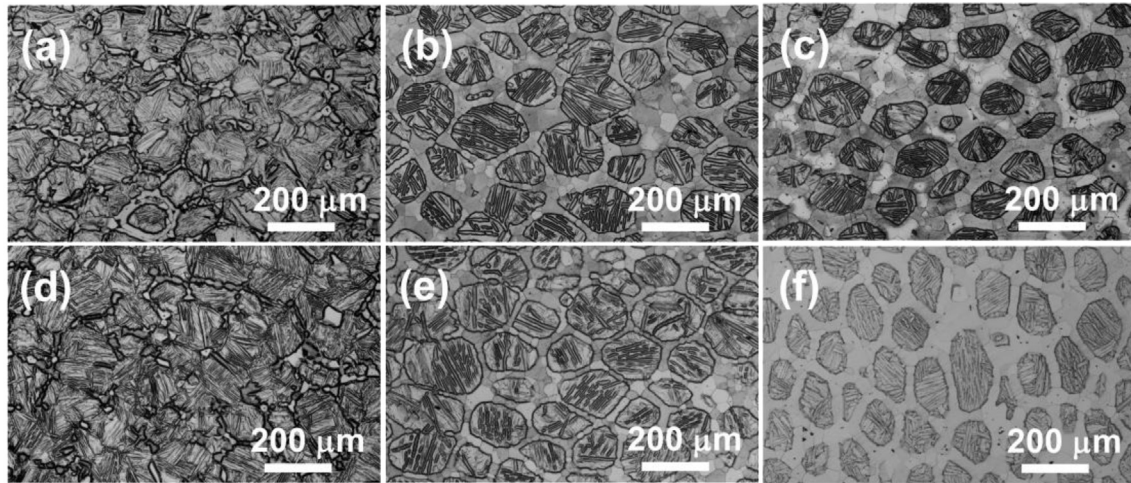
Fig. 2. Optical images of sintered compacts subjected to annealing at 1000 °C (a–c), 1100 °C (d–f) for Ti-900-15 (a, d), Ti-1000-15 (b, e), Ti-1000-30 (c, f), respectively.

unlike the case in tantalum, where a composition gradient without any sharp boundary is formed within a grain [12,13].

Figs. 2 and 3 shows the optical images of the sintered Ti-900-15, Ti-1000-15 and Ti-1000-30 specimens annealed at different temperatures. It can be seen the CS structure, especially the shell thickness has an obvious change against the annealing temperature T varying from 1000 °C to 1500 °C. Fig. 3d summarizes the shell area fraction, A_s, versus T. After annealing at 1000 °C, A_s increases from 6%, 21%, 36%–11%, 40%, 51% for Ti-900-15, Ti-1000-15 and Ti-1000-30 respectively. Further increasing T reduces A_s continuously for all the three samples. For Ti-1000-15 and Ti-1000-30, $A_s = 37\%$ and 47% respectively when $T = 1100$ °C. Then the shell networks tend to be non-continuous at 1300 °C (Fig. 3b and c) and disappears completely when $T = 1500$ °C (Fig. 3e and f). As for Ti-900-15, the network architecture remains discontinuous after annealing at 1000 °C (Fig. 2a) and 1100 °C (Fig. 2d), then disappears completely as the annealing temperature reaches 1300 °C, replaced by a homogeneous coarsened lamellar structure, as shown in Fig. 3a.

Further prolonged annealing time at different temperatures doesn't change the annealed microstructures, as exemplified in Fig. 4a for Ti-1000-15 annealed at 1000 °C for 10 h, indicating that the sample approaches a stable status after 1 h annealing. The

above shell thickness changes versus annealing temperature phenomena can be well understood on the basis of the phase diagram in Fig. 4b [14]. In term of the lever rule, the weight percentage of α-Ti shell (X_α) can be expressed in Eq. (1):

$$X_\alpha = \frac{W - W_\beta}{W_\alpha - W_\beta} \tag{1}$$

where W, W_β, and W_α represent the N atomic percents in Ti alloy, β-Ti and α-Ti, respectively. It can be seen that with an increase in temperature, $W-W_\beta$ is reduced, while $W_\alpha-W_\beta$ is increased obviously, resulting in a sharp reduction of X_α. So it is reasonable to observe a decreased A_S with increasing T. The short time of SPS sintering process caused an incomplete N diffusion in the as-sintered Ti-N alloys, and subsequent annealing at 1000 °C for 1 h enhanced the N diffusion and therefore increased the shell thickness.

Typical compressive true stress–strain curves of the SPS sintered CP Ti and CS Ti-N alloys as well as annealed specimens are shown in Fig. 5a. The as-sintered CS Ti alloys display significantly enhanced yield strength σ_s with obvious strain hardening phenomenon after yielding. For instance, for Ti-900-15 specimen, σ_s is 0.9 GPa, about 2.2 times as large as that of the sintered CP Ti
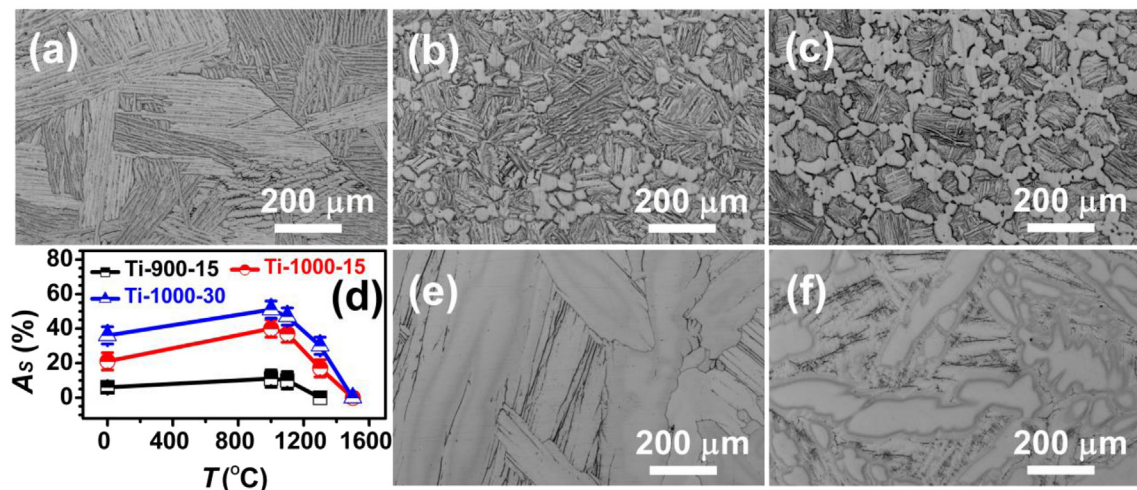
Fig. 3. Optical images of sintered compacts subjected to annealing at 1300 °C (a–c) and 1500 °C (e, f) for Ti-900-15 (a), Ti-1000-15 (b, e), Ti-1000-30 (c, f), respectively. Variations of area fraction of shell A_s versus annealing temperature T are summarized in (d).
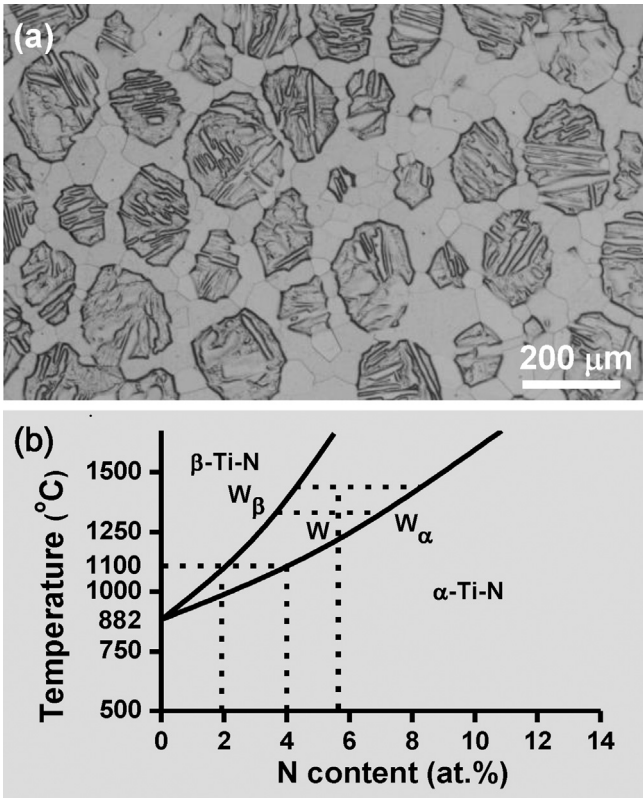
Fig. 4. (a) Optical images of Ti-1000-15 subjected to annealing at 1000 °C for 10 h, (b) schematic representation of the partial Ti-N phase diagram [14].

(0.4 MPa), and the flow stress increased from 0.9 to 1.2 GPa at the strain of 13%. Moreover, annealing at 1000 °C further enhanced σ_s without sacrificing fracture plasticity ε_f. σ_s was increased noticeably from 0.9 GPa, 1.1 GPa, 1.17 GPa–1 GPa, 1.4 GPa, 1.44 GPa for Ti-900-15, Ti-1000-15, Ti-1000-30 respectively without the any loss in plasticity. Fig. 5c–e summarizes the corresponding σ_s and ε_f. With a further increment in T over 1000 °C, σ_s was reduced gradually while ε_f was kept constant. When $T = 1500$ °C, ε_f dropped dramatically to 2.8% and 1.8% for Ti-1000-15 and Ti-1000-30, respectively. The σ_s variations as a function of A_S are plotted in Fig. 5b. It can be seen the higher A_S, the higher σ_s, implying the superior strengthening effect can be attributed to the continuous Ti-N networks.

Considerable solid solution strengthening of pure titanium by incorporating interstitials in its lattice has been well documented [15], even with dilute contents less than 1 at.%. So it is clear that the high strength of compacts is in part a direct consequence of solid solution strengthening of nitrogen. Another part of the strengthening came from deformation limit of the Ti-N shell to the soft Ti core. In terms of Hashin-Shtrikman (H-S) theorem [16], the hard phases can strengthen a material up to the hilt only when they enclose the soft phases continuously. So the CS Ti can be considered reasonably as the one with H–S upper bound structure [16], which maximally realize the solid solution strengthening of nitrogen. This can be further confirmed by the lateral morphologies where the Ti-N shell blocks the propagation of shear bands and confines the shear bands within the individual soft Ti cores (Fig. 6a), in comparison with shear bands extending to different grains for the CP Ti, as shown in Fig. 6b.

The ductility of Ti with interstitial dissolved oxygen or nitrogen is usually disappointingly low although exhibiting enhanced strength. For example, for titanium containing 0.8 wt% or nitrogen of 0.4 wt%, its ability of plastic deformation disappears completely [15]. Several investigations have shown that a high compression fracture strain was obtained in a commercial pure Ti with high
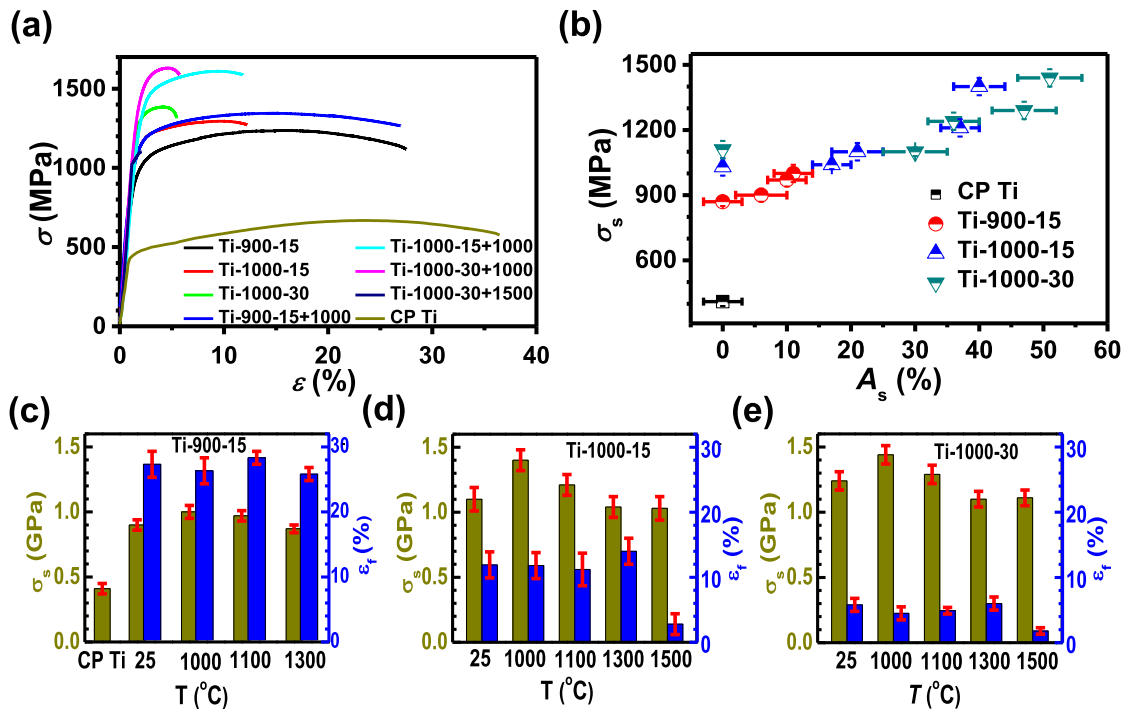
Fig. 5. (a) Typical compressive stress–strain curves of the SPSed CP Ti, Ti-N alloy and annealed Ti-N specimens. (b) Variations of yield strength σ_s versus the shell area fraction A_s for the three sintered compacts and CP Ti with and without annealing. (c)–(e) Annealing temperature T dependences of the yield strength σ_s and fracture plasticity ε_f of (c) Ti-900-15, (d) Ti-1000-15, (e) Ti-1000-30.
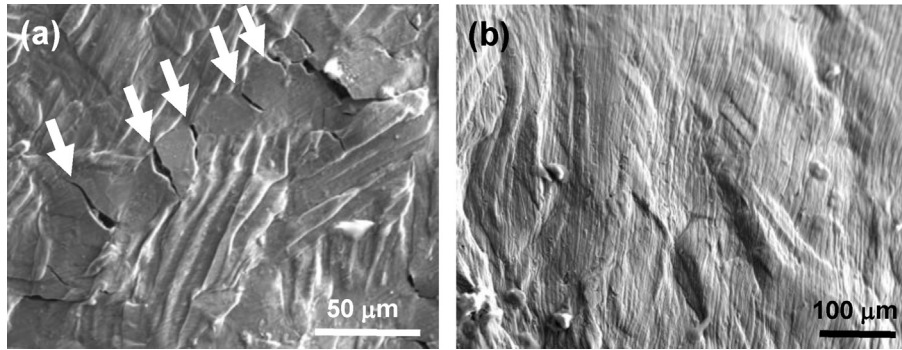
Fig. 6. Cross-sectional SEM images of the compressed (a) Ti-900-15 annealed at 1000 °C for 1 h and (b) conventional CP Ti.

interstitial contents of 1.34 wt% O and 0.3 wt% N, which is believed to stem from non-equilibrium grain boundary configuration and the bimodal grain structure [17]. In the present study, a high plasticity is also obtained along with high strength. It is likely that the achievement of a certain degree of plastic strain in the Ti-N alloys comes from the soft grain center, where moderate strain hardening is retained due to solid solution of only a paucity of nitrogen. The soft cores may help dissipate deformation strains and absorb energy, improving the plasticity. A great number of microcracks were distributed in the Ti-N shells (Fig. 6a) suggesting that cracks were nucleated first within the Ti-N shell regions, and were blunted or impeded by the soft Ti cores (indicated by arrows), resulting in the moderate fracture plasticity. It is similar to the case for laminated composites with a strong interface between a Cu layer and Al layer [18].

With an increasing N content as well as shell thickness, the CS Ti alloys exhibit an increasing strength and a decreasing plasticity (Fig. 5). The peculiar microstructure of high strength shells encapsulating soft cores discontinuously, which can make full use of their advantages, enables Ti-900-15 an excellent strength-plasticity synergy. The strengthening effect is weakened slightly as the networked CS structure is partly broken (Fig. 1a). While the continuous and interpenetrating matrix phase endows Ti-900-15 with a striking plasticity. The beneficial effects of interpenetrating matrix in bearing the strain, blunting the crack and decreasing the crack-propagation speed have been reported in TiB whiskers reinforced Ti matrix composites [19,20].

For the sample subjected to different annealing temperatures, the O and N contents are deemed to be unchanged because Ti has a strong affinity these elements [21]. So the mechanical performances can be related directly to the changes in microstructure. σ_s is testified to follow a linear relationship with A_S (Fig. 5b), indicating the strongly strengthening role of the shells. In addition, annealing at high temperatures will further improve the metallurgical bonds between different grains, which is beneficial for plasticity. Therefore, after annealing at temperatures below 1500 °C, the CS Ti alloys exhibited superior mechanical properties with high strength and good plasticity. For Ti-1000-15 and Ti-1000-30 annealed at 1500 °C, the Ti-N shell was destroyed and the N content is high enough to embrittle the whole specimen, leading to the catastrophic fracture.

4. Conclusions

Bulk dense titanium compacts with three different N contents and a 3-D networked CS structures were synthesized successfully by means of spark plasma sintering (SPS) of the nitrided titanium particles. The area fraction of the Ti-N shell (A_S) and yield strength (σ_s) increase with an increasing N content, accompanying with the decrease of the fracture plasticity. During annealing, A_S and σ_s

increased first at annealing temperature of 1000 °C, then decreased gradually with further increasing annealing temperatures. Fracture plasticity keeps unchanged during annealing except a dramatic drop at annealing temperature of 1500 °C. A linear relationship is observed between σ_s and A_S indicating the hardening effect of the Ti-N shell.

References

[1] K. Wang, The use of titanium for medical applications in the USA, Mater. Sci. Eng. A 213 (1996) 134—137.
[2] R.R. Boyer, An overview on the use of titanium in the aerospace industry, Mater. Sci. Eng. A 213 (1996) 103—114.
[3] X.L. Wu, M.X. Yang, F.P. Yuan, G.L. Wu, Y.J. Wei, X.X. Huang, Y.T. Zhu, Heterogeneous lamella structure unites ultrafine-grain strength with coarse-grain ductility, Proc. Natl. Acad. Sci. U. S. A. 112 (2015) 14501—14505.
[4] D.K. Yang, P. Cizek, D. Fabijanic, J.T. Wang, P.D. Hodgson, Work hardening in ultrafine-grained titanium: multilayering and grading, Acta Mater. 61 (2013) 2840—2852.
[5] C. Brozek, F. Sun, P. Vermaut, Y. Millet, A. Lenain, D. Embury, P.J. Jacques, F. Prima, A β-titanium alloy with extra high strain-hardening rate: design and mechanical properties, Scr. Mater. 114 (2016) 60—64.
[6] T.H. Fang, W.L. Li, N.R. Tao, K. Lu, Revealing extraordinary intrinsic tensile plasticity in gradient nano-grained copper, Science 331 (2011) 1587—1590.
[7] X.L. Wu, P. Jiang, L. Chen, F.P. Yuan, Y.T. Zhu, Extraordinary strain hardening by gradient structure, Proc. Natl. Acad. Sci. U. S. A. 111 (2014) 7197—7201.
[8] B.X. Liu, L.J. Huang, L. Geng, B. Wang, C. Liu, W.C. Zhang, Fabrication and superior ductility of laminated Ti—TiBw/Ti composites by diffusion welding, J. Alloy. Compd. 602 (2014) 187—192.
[9] T. Aydogmus, Processing of interpenetrating Mg-TiNi composites by spark plasma sintering, Mater. Sci. Eng. A 624 (2015) 261—270.
[10] L.J. Huang, L. Geng, H.-X. Peng, Microstructurally inhomogeneous composites: is a homogeneous reinforcement distribution optimal, Prog. Mater. Sci. 71 (2015) 93—168.
[11] Y.S. Zhang, Y.H. Zhao, W. Zhang, J.W. Lu, J.J. Hu, W.T. Huo, P.X. Zhang, Core-shell structured titanium-nitrogen alloys with high strength, high thermal stability and good plasticity, Sci. Rep. 7 (2017) 40039.
[12] Y.S. Zhang, X.M. Zhang, G. Wang, X.F. Bai, P. Tan, Z.K. Li, Z.T. Yu, High strength bulk tantalum with novel gradient structure within a particle fabricated by spark plasma sintering, Mater. Sci. Eng. A 528 (2011) 8332—8336.
[13] Y.S. Zhang, X.M. Zhang, X.F. Bai, P. Tan, F.C. Dong, Z.K. Li, Z.T. Yu, Effect of thermal annealing on microstructure and mechanical properties of a gradient structured tantalum prepared by plasma activated sintering, Int. J. Refract. Met. Hard Mater. 30 (2012) 1—5.
[14] E. Etchessahar, J.P. Bars, J. Debuigne, The Ti-N system: equilibrium between the δ, ε and α phases and the conditions of formation of the lobier and marcon metastable phase, J. Less Common Met. 134 (1987) 123—139.
[15] H. Conrad, Effect of interstitial solutes on the strength and ductility of

titanium, Prog. Mater. Sci. 26 (1981) 123–403.

[16] Z. Hashin, S. Shtrikman, A variational approach to the theory of the elastic behaviour of multiphase materials, J. Mech. Phys. Solids 11 (1963) 127–140.

[17] W. Xu, X. Wu, D. Sadedin, G. Wellwood, K. Xia, Ultrafine-grained titanium of high interstitial contents with a good combination of strength and ductility, Appl. Phys. Lett. 92 (2008) 011924.

[18] H.S. Liu, B. Zhang, G.P. Zhang, Delaying premature local necking of high-strength Cu: a potential way to enhance plasticity, Scr. Mater. 64 (2011) 13–16.

[19] L.J. Huang, F.Y. Yang, H.T. Hu, X.D. Rong, L. Geng, L.Z. Wu, TiB whiskers reinforced high temperature titanium Ti60 alloy composites with novel network microstructure, Mater. Des. 51 (2013) 421–426.

[20] L.J. Huang, S. Wang, Y.S. Dong, Y.Z. Zhang, F. Pan, L. Geng, H.X. Peng, Tailoring a novel network reinforcement architecture exploiting superior tensile properties of in situ TiBw/Ti composites, Mater. Sci. Eng. A 545 (2012) 187–193.

[21] T.H. Okabe, R.O. Suzuki, T. Oishi, K. Ono, Thermodynamic properties of dilute titanium-oxygen solid solution in beta phase, Mater. Trans. 32 (1991) 485–488.